Measurement 166 (2020) 108087

Contents lists available at ScienceDirect

Measurement

journal homepage: www.elsevier.com/locate/measurement

A novel velocity anisotropy probability imaging method using ultrasonic guided waves for composite plates

Yuan Liu, Xiaobin Hong *, Bin Zhang

School of Mechanical and Automotive Engineering, South China University of Technology, Guangzhou 510641, People's Republic of China

ARTICLE INFO

Article history:
Received 3 February 2020
Received in revised form 22 April 2020
Accepted 6 June 2020
Available online 27 June 2020

Keywords:
Anisotropic composite
Ultrasonic guided waves
PZT
Damage identification
Velocity anisotropy probability imaging

ABSTRACT

Due to its excellent performance, composite materials are widely used in engineering structures. However, because of the velocity anisotropy, it is difficult to detect the damage accurately. In this paper, a novel velocity anisotropy probability imaging method is developed. Firstly, the velocity in all directions is obtained through numerical simulation technique. Secondly, the model of velocity anisotropy composite plates is established. The damage probability is determined by time coefficient (C_T) and damage sensitive index (DSI). Then, experiments with different damage states are carried out. The results show that the damage information can be displayed accurately, and it's clearer by applying a threshold of 90%. The probability of crack tips is higher than that of the middle, which reflects the influence of crack on the received signal. The sum of damage sensitive index (DSI_{sum}) increases with the damage degree, which indicates the damage severity. This method can successfully detect the damage.

1. Introduction

Composite materials have the advantages of high specific strength, high specific modulus, corrosion resistance, easy processing and molding by combining materials with different properties. Because of its excellent comprehensive performance, composite materials are widely used in aerospace, shipbuilding, automotive, pipeline transportation and other fields. Especially in aerospace and shipbuilding, it is very helpful to reduce the weight of the structure. However, the physical properties of different materials are quite different, and various damage such as cracks and delamination may occur during manufacturing and applications. The structural integrity of composite materials is destroyed for the existence of the defects, and its comprehensive performance declined severely. Therefore, damaged detection and monitoring of composite materials has always been a research hotspot in structural health.

Ultrasonic guided waves can propagate for a long distance and remain the sensitivity to many kinds of defects, which shows great potential in nondestructive testing field. Recent years, ultrasonic guided waves damage detection imaging method have attracted much attention because they can intuitively reflect the information of damage. At present, commonly used ultrasonic imaging methods including phased array imaging method, delay-and-sum imaging method and probability imaging method. Phased array technology can focus in a certain space by controlling the phase and amplitude of each element of the transducer array, so as to scan the structure and reconstruct the damage status of the structure. Vishnuvardhan et al. [1] applied single-transmitter multiple-receiver array to achieve the large areas detection of plate-like structures, and the adopted phased addition algorithm can reconstruction the defects information accurately. Yu et al. [2] designed a rectangular transducer array to receive guided wave signals from all directions, and developed a generic beamforming algorithm for the detection of a thin wall structures. Hall et al. [3] provided a rapid and low-cost ultrasonic guided waves damage imaging method using a distributed array. Tian et al. [4] located and quantified damage of composite material by combined phased array and non-contact laser vibrometer which could reduce most of detection time, and its results were verified by C-scan. However, the accuracy of phased array method is greatly affected by the number of transducers. Delay-and-sum method can achieve the structural damage detection and imaging using sparse transducer array, which greatly reduces the number of sensors. Hall et al. [5] improved the computational efficiency of delay-and-sum imaging method through matrix inversion optimization which reduced the computational complexity of the imaging algorithm. Sharif-Khodaei et al. [6] proposed an improved delay-and-sum method through windowed energy arrival of received guided waves signal for the inspection of composite plates structure, and showed the damage location in pictures with only four transducers. Lu et al.

* Corresponding author.
E-mail address: mexbhong@scut.edu.cn (X. Hong).

https://doi.org/10.1016/j.measurement.2020.108087
0263-2241/

[7] presented a multipath delay-and-sum method based on sparse transducers with only one excitation, and both ellipses and hyperbolas imaging were applied to accurate show the damage information of aluminum alloy plate. However, the delay-and-sum imaging method needs precise time control to present accurate damage results.

Probability imaging method can achieve high-quality damage imaging with fewer sensors by accumulating the damage index of different paths. Wang et al. [8] estimated the probability of aluminum plates using the correlation coefficients between the damaged signal and no-damaged signal. Hettler et al. [9] applied baseline-dependent and baseline-independent probability imaging method to detect the impact damage of composite structures. Li et al. [10] studied the robustness of the probabilistic imaging method for the detection of plate-like structure. The damage probability in the above literature changes linearly according to the damage index and the distance between the imaging point and the sensing path. That is to say, whether the actual damage is located in the sensor path or not, the probability is always largest on the sensing path. This is obviously unreasonable. Therefore, the probability imaging method based on ellipse is proposed to improve the imaging quality. Zhao et al. [11] presented a fusion ellipse probability imaging method by extract multi features such as flight time, energy and correlation to enhance the reliability of the imaging results. Su et al. [12] developed a nonlinear ultrasonic guided waves damage inspection method, and the nonlinearity coefficient was used as damage index in the ellipse probability imaging. Liu et al. [13] exacted nonlinear Lyapunov damage index through Duffing chaotic oscillator to show the delamination defect using ellipse probability imaging method. Zeng et al. [14] improved the quality of elliptical-based probability imaging by adding a virtual transducer with as few sensors as possible. However, when the ellipse probability imaging technology is applied to anisotropic materials, the imaging result is not good as that of isotropic materials, which is also reflected in some of the above literatures [12,14]. For this problem, Moll et al. [15] proved that the damage location of anisotropic materials can not solved analytically, and the spectral element method is used in his paper to solve the problem numerically. Kundu et al. [16] transformed the problem into a minimum error function to obtain the impact position. Of course, both methods require complex calculations and principles.

On the other hand, lead zirconate titanate (PZT) is the most popular ultrasonic transducer because of its low cost, small size and excellent ultrasonic performance. PZT can be used as either an actuator or a receiver through the positive and negative piezoelectric effect. Sethi et al. [17] developed a pole placement controller to control the multi-mode vibration of guided waves using PZT as actuator and receiver. Jang et al. [18] prepared PZT films and tested its excitation and sensing properties. Shen et al. [19] established a predictive modeling of nonlinear wave propagation using PZT as active sensors. Wang et al. [20] studied the virtual time reversal algorithm to eliminating the dispersive multi-mode of Lamb wave through PZT array. PZT is not limited by the type of damage and is sensitive to many kinds of damage. Peter et al. [21] applied PZT as ultrasonic sensing element to achieve quantitative characterization of gas pipeline corrosion damage. Parvasi et al. [22] monitored the tightness of bolt connection through a PZT to excite and another received on the other side, and found that wave energy increased with bolt preload. Jiang et al. [23] successfully detect the fatigue damage through an active PZT sensing mode. PZT can effectively exciting and receiving ultrasonic signals from various materials, including both metal and non-metal materials. Hong et al. [24-28] utilized PZT as the ultrasonic transducer to detect many kinds of damage of glass, plastic, messenger cable and porcelain. Luo et al. [29] evaluated the quality of concrete by measure the propagation time of guided waves using PZT. Therefore, a sensor network composed of PZT transducers is used to excite and receive guided wave signals.

The anisotropy and non-uniformity of the composite material cause the guided wave mode to be very complicated, and the velocity in all directions is different. This makes the probability imaging result inaccurate or even completely wrong. Therefore, it is of great valuable to realize damage imaging of anisotropic materials through simple calculation. In this paper, a novel ultrasonic guided waves probability imaging method is developed by using the velocity in all directions of anisotropic composite plates. The overall framework of this paper is as follows. Firstly, the dispersion characteristic of anisotropic composite plates is introduced, and the probability imaging method based on velocity in all directions is present. Then, the difference between the guided wave signals of damaged and non-damaged composite plates is analyzed by finite element simulation technique, and the imaging characterization is carried out. Finally, the experiment platform is established to verify the simulation results.

2. Theory and methodology

2.1. Theoretical foundation of anisotropic composite plates

两个坐标系

Two coordinate systems are needed to solve the problem of guided waves propagation in anisotropic materials, one is to define the coordinate system of materials and the other is to describe the wave propagation and vibration, which is shown in Fig. 1.

In cartesian coordinates (x, y, z), there are 9 elastic coefficients of orthotropic materials, which are represented by a fourth order tensor C_{ijkl}, and its matrix form is as follows:

$$C_{ijkl} = \begin{bmatrix} C_{11} & C_{12} & C_{13} & 0 & 0 & 0 \\ C_{12} & C_{22} & C_{23} & 0 & 0 & 0 \\ C_{13} & C_{23} & C_{33} & 0 & 0 & 0 \\ 0 & 0 & 0 & C_{44} & 0 & 0 \\ 0 & 0 & 0 & 0 & C_{55} & 0 \\ 0 & 0 & 0 & 0 & 0 & C_{66} \end{bmatrix} \tag{1}$$

In Cartesian coordinates (x', y', z'), the elastic constant is calculated according to the transformation formula:

$$C_{mnop} = \beta_{mi}\beta_{nj}\beta_{ok}\beta_{pl}C_{ijkl}, (m,n,o,p,i,j,k,l = 1,2,3) \tag{2}$$

Where β_{ab} is the direction cosine between coordinate axis x and x′, the form of transition matrix β is as follows:

$$\beta_{ab} = \begin{bmatrix} \cos\beta & \sin\beta & 0 \\ -\sin\beta & \cos\beta & 0 \\ 0 & 0 & 1 \end{bmatrix} \tag{3}$$

Substituting equations (1) and (3) into equation (2), the elastic coefficient matrix in coordinate system (x', y', z') is obtained as follows:

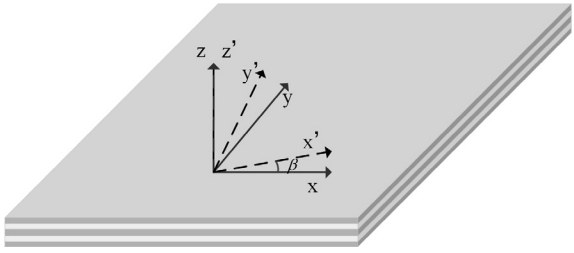

Fig. 1. Coordinate diagram of multiplayer anisotropic composite plate.

$$C_{mnop} = \begin{bmatrix} C'_{11} & C'_{12} & C'_{13} & 0 & 0 & C'_{16} \\ C'_{12} & C'_{22} & C'_{23} & 0 & 0 & C'_{26} \\ C'_{13} & C'_{23} & C'_{33} & 0 & 0 & C'_{36} \\ 0 & 0 & 0 & C'_{44} & C'_{45} & 0 \\ 0 & 0 & 0 & 0 & C'_{55} & 0 \\ C'_{16} & C'_{26} & C'_{36} & 0 & 0 & C'_{66} \end{bmatrix} \quad (4)$$

When the propagation direction is along the x-axis, the two coordinate systems coincide, the matrix form of stiffness coefficient is as equation (1), and when the propagation direction is in other directions, the matrix form of stiffness coefficient is as equation (4). Therefore, in different directions of the anisotropic composite plates, the dispersion curves obtained by the stiffness coefficient matrix are quite different. That is to say, the wave sve-locities in all directions are different.

wave's velocities

2.2. Anisotropic velocity of composite plates

Velocity of the guided waves is the most important factor in damage detection and imaging. However, the anisotropy of composite materials causes great trouble to the damage detection and imaging. To obtain the damage information more accurately, the velocity in all directions of the anisotropic composite plate is needed. On the other hand, the process of solving the anisotropic composite plate dispersion curve is very complicated, and it needs to be calculated in all direction. The theoretical calculation always deviates from the actual situation. Therefore, in this paper, finite element simulation software ABAQUS (Abaqus Inc., CA, USA) is adopted to obtained the velocity in all direction.

A carbon fiber reinforced composite plate with 0/90 ply orientation is considered. The size of the plate is 600 mm × 600 mm × 3 mm and the number of layers is 15. The performance parameters of composite plate are shown in table 1. The dispersion curve of the composite plate along the 0° direction is shown in Fig. 2. It can be seen that the velocity of guided waves in the range of 60–300 kHz is almost non-dispersive. Therefore, a 200 kHz 5-peak sine wave which modulated by a Hanning window is selected as the excitation signal. In this frequency range, the S_0 mode is the fastest and almost no dispersion. Therefore, it is used to calculate the propagation time of guided waves in this paper.

激发频率

The simulation model of the composite plate is shown in Fig. 3. To match the actual situation, the PZT which used as the ultrasonic transducer is also simulated. The excitation transducer is located in the center of the plate, and 17 receiving transducers are located in the first quadrant because of the symmetry, and evenly distributed on the circle 20 cm from the excitation. All the transducers are constraint on the plate using the "Tie" function. A Dynamic Explicit step is created for the solution of the model, and the time is set to be 0.0003 s. Eight nodes on four corners of the composite plate are set with completely fixed constraints. To simplify the model and simulate the vibration effect of PZT, the uniform pressure is applied on the exciting PZT. The element type of the composite plate is an 8-node quadrilateral in-plate general-purpose continuum shell (SC8R). It is noticed that, the length width ratio of grid element should not be too much, otherwise the calculation result will be inaccurate. The in-plane stress of the node in the center of PZT transducers is extracted as the received guided waves signal.

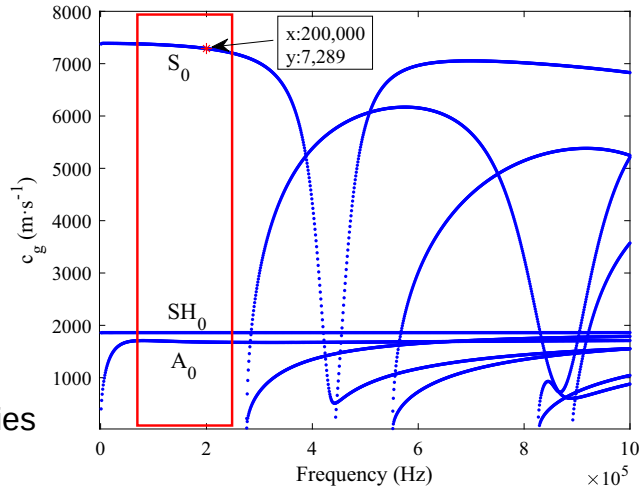

Fig. 2. The dispersion curve of the composite plate along the 0° direction.

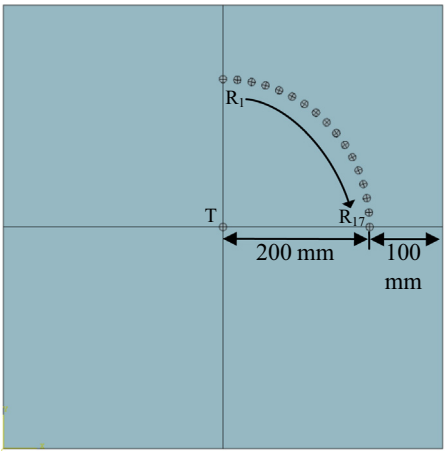

Fig. 3. The distribution of the PZT array in the simulation of velocity.

8度多项拟合

Fig. 4 (a) shows the received signals from PZT R_1 to R_9. When the signal is greater than a threshold (1×10^{-3} is taken in this paper), it is determined as the arrival time of the wave. The calculated wave velocity is fitted by 8-degree polynomial, and the group velocity of anisotropic composite plate in all directions is obtained as shown in Fig. 4 (b). It can be seen that, the received signal of each transducer is different due to anisotropy, and the arrival time also becomes longer as it deviates from 0° or 90°. The velocity in the direction of 0° is calculated as 6969 m / s, which is close to the result in Fig. 2. The velocity is the fastest when the angle of propagation is parallel to the ply direction. The larger the Angle between the propagation direction and the ply direction, the slower the velocity of the guided waves will be. This is consistent with the characteristic of the composite plates, and similar results have been found in other literatures [30-32]. The obtained velocity can be used for the velocity anisotropy probability imaging.

Table 1
The performance parameters of composite plate.

E_1/GPa	E_2/GPa	G_{12}/GPa	G_{23}/GPa	N_u	ρ/kg·m^{-3}
144.7	9.65	9.65	3.4	0.3	1500

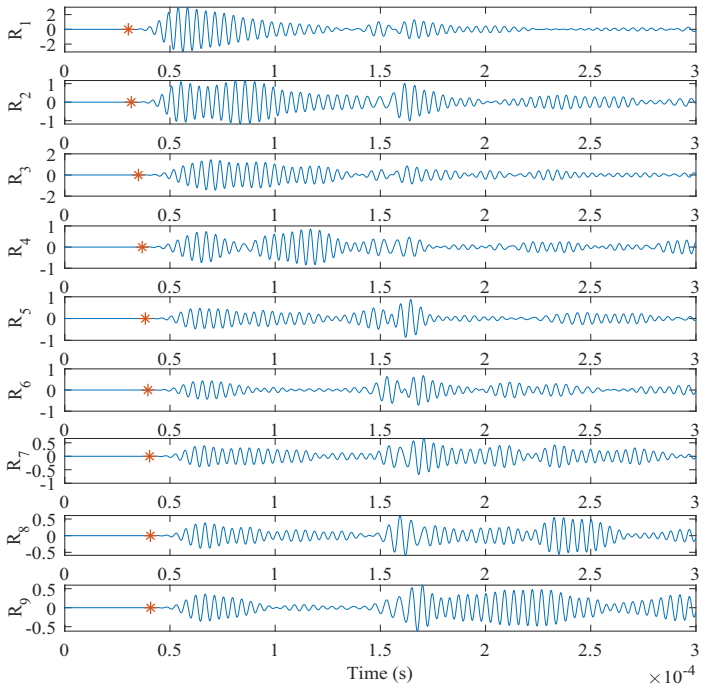

(a) The received signals from PZT R_1 to R_9.

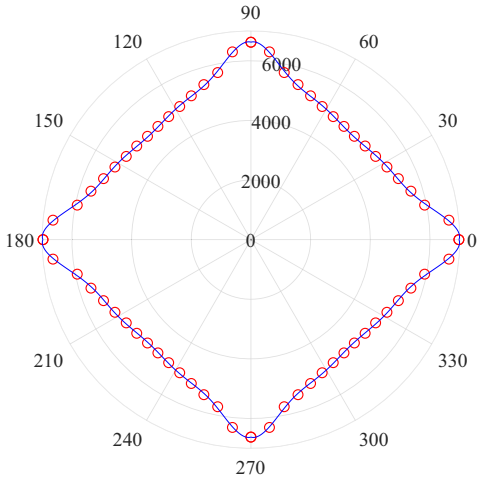

(b) Group velocity in all directions after fitting.

Fig. 4. The simulation result of anisotropic composite plate with 0/90 ply.

2.3. Probability imaging method based on velocity anisotropy

(1) Time coefficient. The difference between damaged and pristine signals is caused by the interaction between guided waves and damage. Ideally, the residual signal obtained by subtracting the two signals will be the scattering signal of the damage [33-35]. The arrival time of the first wave packet of the scattering signal is the time when the excitation signal reaches the receiver after the damage reflection. Then, the time difference of arrival time between the pristine and damaged signals can be calculated. For isotropic materials, the velocity in all directions is the same. According to the time difference, the propagation distance of the signal from the actuator to the receiver after damage scattering is a fixed value, and the damage is determined on an ellipse. This method has been used in many literatures and good results have been obtained [11,36,37]. However, due to the different velocities in anisotropic materials, the damage does not lie on a standard ellipse. The imaging results are not very accurate or even wrong using a same velocity. Moreover, the different velocities make it almost impossible to calculate the location of the damage. Therefore, another strategy is adopted to calculate the damage probability of composite plates in the paper.

Consider an anisotropic composite plate with N transducers as transmitter or receiver, and $N \times (N-1)$ different paths are generated. Take one path as an example, transmitter and receiver are located at (x_T, y_T) and (x_R, y_R) and a damage located at (x_D, y_D), as shown in Fig. 5. The distances between transmitter, receiver and damage can be obtained by:

$$\begin{aligned} L_{TR} &= \sqrt{(x_R - x_T)^2 - (y_R - y_T)^2} \\ L_{TD} &= \sqrt{(x_D - x_T)^2 - (y_D - y_T)^2} \\ L_{DR} &= \sqrt{(x_R - x_D)^2 - (y_R - y_D)^2} \end{aligned} \tag{5}$$

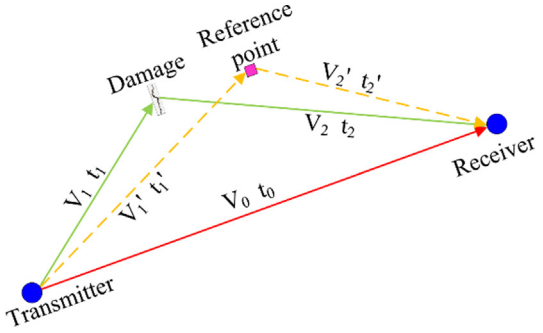

Fig. 5. Schematic diagram of damage detection in anisotropic composite plate.

Because of the S0 mode is the fastest and almost no dispersion which showed in Fig. 2. Therefore, it is used to calculate the propagation time of guided waves. For given velocities, the corresponding time required for the guided waves to travel at each distance is

$$t_0 = \frac{L_{TR}}{v_0}, t_1 = \frac{L_{TD}}{v_1}, t_2 = \frac{L_{DR}}{v_2} \tag{6}$$

Therefore, the time difference of arrival time between the signal received directly and after damage scattering is equal to $\Delta t = t_1 + t_2 - t_0$. According to Δt, the specific location of the damage cannot be determined because of the anisotropic velocity.

Then, the area to be detected is discretized and one of them is taken as the reference point. After the velocity in all directions is obtained, the propagation time between the excitation, reception and reference points can be calculated. Then, the difference of time between damage and reference point can be obtained. Considering the problem of dimension, the basic time t_0 is introduced. The damage probability is closely related to the time difference. Then the time coefficient C_T is defined as:

$$C_T = \frac{\Delta t' - \Delta t}{t_0} = \frac{(t_1' + t_2' - t_0') - (t_1 + t_2 - t_0)}{t_0} \quad (7)$$

Obviously, when $C_T = 0$, the probability of damage at the reference point is the largest. The larger the C_T, the farther the reference point is from the damage, and the lower the damage probability. It should be noted that due to symmetry, there will also be a mirror damage location on the other side of the path, which is incorrect. In addition, when the damage is on the path, the damage probability of all reference points on the path is the same. The damage is finally determined by the cumulative probability of all path.

(2) Damage sensitive index. The difference caused by the interaction of guided wave and damage can be represented by scattering signal. For one path, the amplitude of the scattering signal can be used to characterize the damage degree. Because the wave velocity and attenuation rate of different paths are different, the process of normalization needs to be performed. Therefore, the damage sensitive index (*DSI*) is expressed as:

$$DSI = \frac{\sum_{k=1}^{N}[S_D(k) - S_B(k)]^2}{\sum_{k=1}^{N}[S_B(k)]^2} \quad (8)$$

完整信号

Where $S_D(k)$ and $S_B(k)$ are damaged signal and pristine signal respectively. N is the length of feature vector.

In addition, for the composite plate of non-damage, the maximum probability should not be judged as damage. When there is no damage, *DSI* of all paths is small. Then, the sum of the damage sensitive index (DSI_{sum}) of all paths is defined as the basis to assess the damage degree of the material and whether there is damage in the material.

$$DSI_{sum} = \sum_{r=1}^{N_P} DSI_r \quad (9)$$

When DSI_{sum} is greater than a damage threshold *DT*, the damage exists in the material, otherwise the material is in a non-damage state. Meanwhile, the larger value of *DT*, the more serious material damage.

(3) Damage Probability. According to C_T and *DSI*, the damage probability of the discretized plate is defined as:

$$P(x,y) = \sum_{r=1}^{N_P} p_r(x,y) = \sum_{r=1}^{N_P} DSI_r \cdot W_r(x,y) \quad (10)$$

Where $p_r(x,y)$ is the estimation probability of damage affect by r_{th} path. N_P is the number of sensor path. $W_r(x,y)$ is the weight determined by C_T:

$$W_r(x,y) = \begin{cases} 1 - \frac{1}{\gamma} \cdot C_T, & C_T < \gamma \\ 0, & C_T \geqslant \gamma \end{cases} \quad (11)$$

Where γ is a scaling coefficient that controls the attenuation speed of the probability. If γ is too small, the probability decays too fast with the increase of C_T, and if it is too large, the discrimination is low. The damage state of composite plates can be obtained by presenting the probability values in the form of image. The most likely location of damage is at the maximum probability. The specific step of the method is shown in Fig. 6.

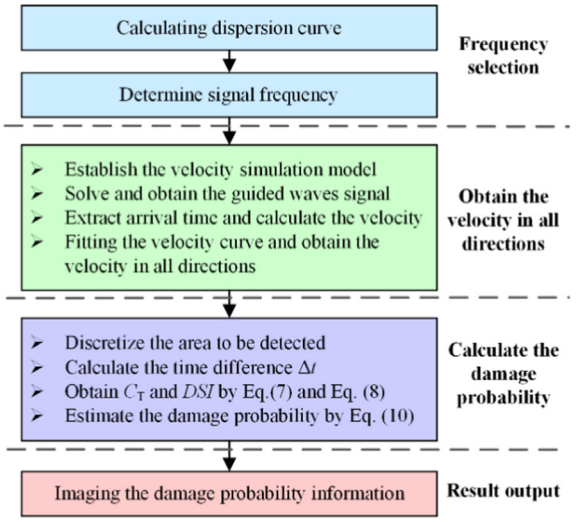

Fig. 6. Flowchart of velocity anisotropy probability imaging method.

3. Numerical simulation

To analyze the influence of damage on guided waves signal, the model including non-damaged and a crack damaged are established for the damage probability imaging. In the center of the plate, the PZT array are evenly distributed on a circle with a diameter of 400 mm, as shown in Fig. 7 (a). The only difference between the two models is the presence of the crack damage. The center of the composite plate model is coordinate origin. The crack is located at (−50 mm, 0 mm) with size 2 mm × 40 mm × 1.8 mm. The mesh model with the crack is shown in Fig. 7 (b). The size of the plate is 600 mm × 600 mm × 3 mm, as same as the velocity simulation. The PZT transducer is successively excited and received by other PZT transducers. The scattering signal is obtained by subtracting the damaged signal and the pristinesignal. Fig. 8 shows the signals received by PZT 2 to 9 when excited by PZT 1. The blue line, orange dash-dotted line and yellow dotted line represent the pristine, damaged and scattering signals.

Theoretically, in isotropic materials, the attenuation rate is the same in all directions, and the signal strength decreases with the increase of distance. However, in anisotropic materials, similar to the velocity, the closer the propagation direction is to the ply orientation of composite plate, the slower the attenuation is, which can been see from Fig. 8. Although PZT 9 is the farthest from the excitation PZT, its signal is the strongest because its propagation direction is the same as that of the ply orientation. In contrast, although PZT 4, 5, 6, 7 and the like are relatively close to the exciting PZT, their propagation direction is significantly different from the material layer direction, and their signals are relatively weak. The signals received by PZT 2, 3, and 4 which located at the left side of the damage are stronger than those of pristine, which means that the excitation signals are received by PZT after the damage reflection. The received signal on the right side of the damage is weaker than that of pristine, that is, the signal is blocked and reflected by the damage during the propagation. Especially, the transition of the signals receiving by PZT 4 and 5 is very obvious because they are on either side of the damage, although they are located in a similar position to the damage.

The received signal is always very complex due to the characteristics of end reflection and dispersion. From Fig. 2, the S_0 mode is the fastest and almost no dispersion, and it is used to calculate the propagation time of guided waves. On the other hand, other modes (e.g. A0), which are similar to S0, will also be affected by damage. In a limited length of data points, A0 and other modes have little influence on the damage sensitivity index. To reduce the interference of other modes as much as possible, the first wave is used in the analysis. Based on the arrival time of pristine signal, the integration of the first 400 data points of scattered signal is taken as the damage sensitive feature using equation (8). Fig. 9 shows the *DSI* of different paths. On path 4T-9R (represents PZT 4 excitation and 9 reception), the value of *DSI* is larger because of the angle between the damage and PZT 4 and 9 are almost parallel to the ply orientation. The wave velocity is also larger on the

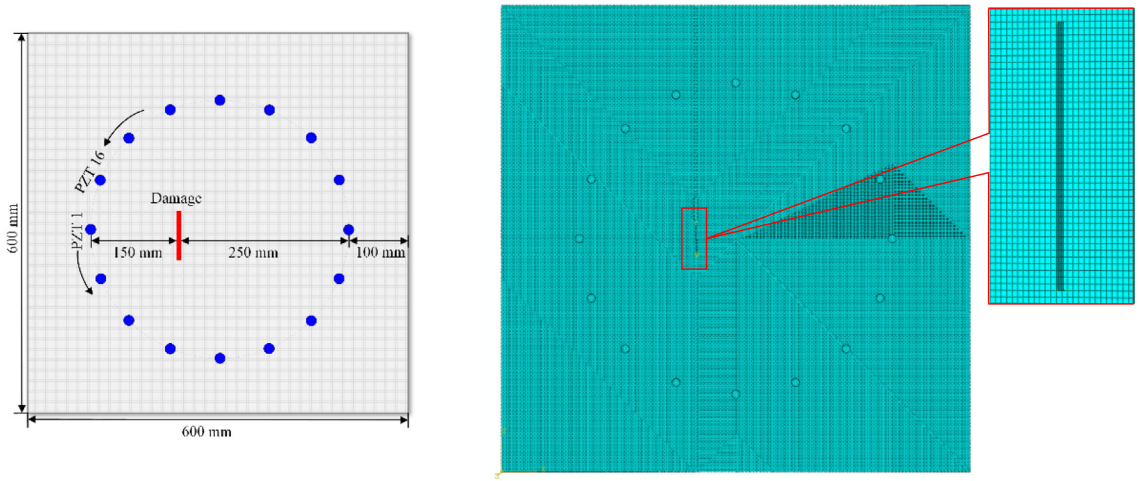

(a) Schematic diagram. (b) The mesh model with the crack.

Fig. 7. The model of anisotropic composite plate.

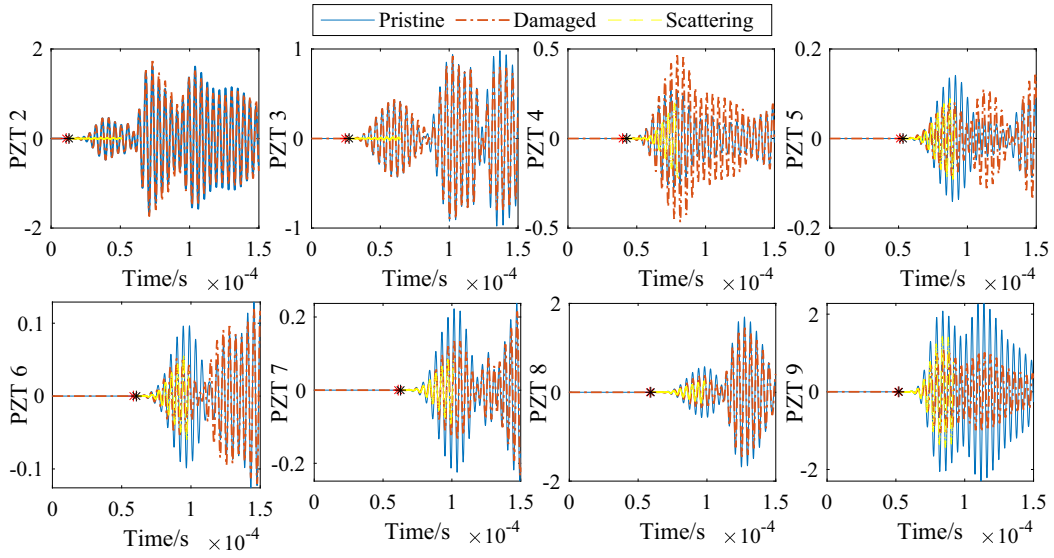

Fig. 8. Signals received by PZT 2 to 9 when excited by PZT 1.

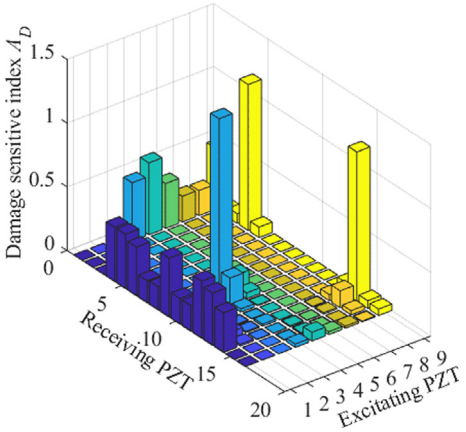

Fig. 9. Damage sensitive index (*DSI*) of different paths.

4T-D-9R path (represents PZT 4 excitation, propagation toward damage and 9 reception). Similarly, on these paths, such as 9T-4R and 9T-14R, the receiving signals are more vulnerable to damage. Obviously, it is wrong to evaluate the damage is located on the path 4T-9R, and it is also inaccurate to evaluate the damage is located on the ellipse around the PZT 4 and 9. The actual location of the damage should continue to expand outward on the basis of ellipse. Therefore, the velocity of anisotropic composite plate in all directions is necessary to obtain accurate imaging results.

The arrival time of the wave is also determined by a threshold 1×10^{-3}, which is the same as the velocity simulation. In Fig. 8, the red and black "*" represent the arrival time of pristine and scattering signals. Table 2 shows the time difference Δt of all paths. When the PZT is both excitation and reception, the value of Δt is set to 0. On paths 1T-9R and 9T-1R, Δt are smallest, because the damage is exactly on the paths. However, in the path away from the damage, such as 1T-4R, 4T-1R, 5T-9R and 9T-5R, Δt is greater. When the excitation and reception of the same path are

Table 2
Time difference Δt of different paths, T and R represent the transmitter and receiver.

$T_D(10^{-6}s)$	1T	2T	3T	4T	5T	6T	7T	8T	9T
1 R	0	6.58	6.58	9.89	3.71	5.40	3.09	2.28	1.91
2 R	6.58	0	5.59	6.98	8.67	9.19	7.20	5.07	4.48
3 R	6.69	5.59	0	5.81	6.58	6.62	4.41	7.20	6.10
4 R	9.08	7.02	5.81	0	6.39	2.39	6.73	9.19	4.19
5 R	4.01	9.00	6.69	6.39	0	6.39	6.58	8.67	11.4
6 R	5.62	7.90	6.73	2.50	6.39	0	5.81	6.98	8.78
7 R	3.31	7.28	4.41	6.73	6.58	5.81	0	5.59	6.28
8 R	2.50	5.07	7.28	7.57	8.89	7.02	5.59	0	6.58
9 R	1.87	2.87	5.51	1.91	11.1	6.98	6.28	6.50	0
10 R	2.50	4.52	6.87	5.11	13.8	9.37	6.39	2.68	6.58
11 R	3.49	8.49	7.09	7.61	12.5	7.50	4.70	6.39	6.69
12 R	5.59	6.80	9.30	11.4	7.68	6.62	7.61	9.37	9.08
13 R	4.01	7.09	9.70	5.37	6.58	9.30	12.5	13.8	12.0
14 R	9.89	9.59	9.11	6.69	5.37	9.89	7.68	5.40	4.41
15 R	6.28	6.28	4.59	9.11	7.31	8.89	6.91	6.73	5.92
16 R	6.58	3.09	6.69	9.70	6.80	6.80	6.62	4.41	4.48

interchanged, the value of Δt does not change much. The positive and negative signal paths between the same pair of transducers are theoretically consistent. The number of signal paths can be reduced to improve the detection efficiency. It is worth noting that the distance between 1T and 4R and 1T-5R is similar, but the difference of Δt is very large. This is because the distance between path 1T-4R and path 1T-5R is shorter but the wave velocity is faster, while the distance and wave velocity between path 1T-D-4R and path 1T-D-5R is not much different. According to equation (7), the C_T of discrete points can be calculated.

Fig. 10 shows the damage probability imaging with different PZT as transmitter when $\gamma = 0.1$. The value of γ is determined by trial and error. The image resolution is 10,000 data points per meter. In Fig. 10 (a), the velocity in all direction is different which means the velocity has been corrected, and velocity in all direction is the same and set to 6969 m/s (velocity in 0° direction) in Fig. 10 (b). That setting the velocity in all directions to be the same is to consider the composite plate as isotropic, and the result is shown as conventional elliptical imaging. Short black lines and circles represent damage and PZT transducers, respectively. It can be seen

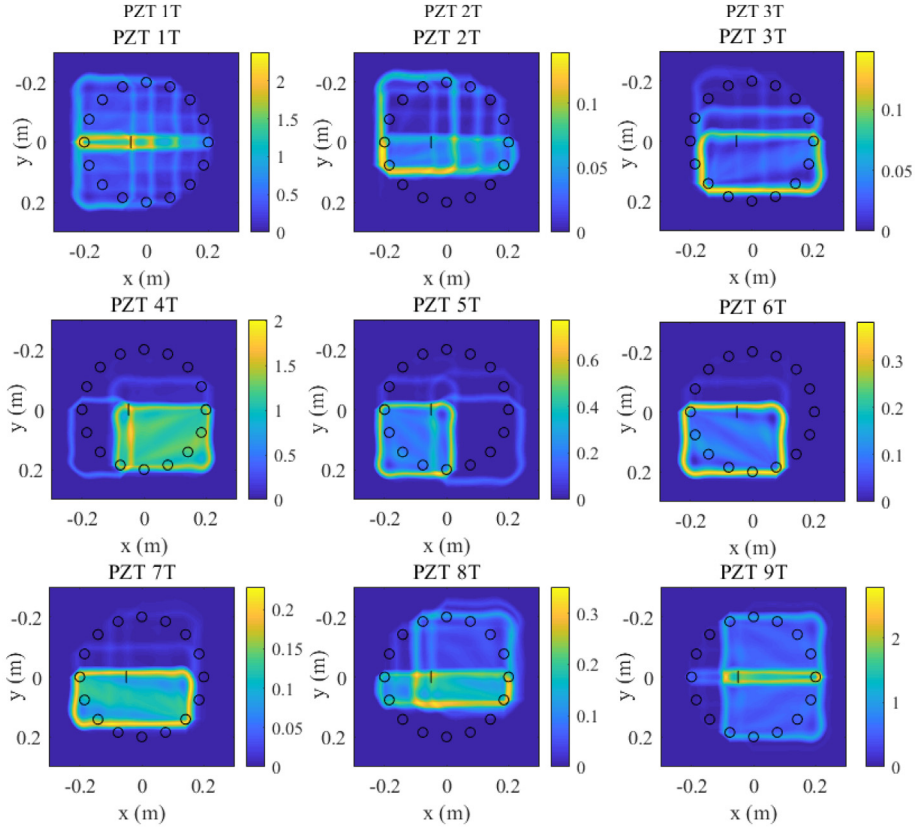

(a) Velocity in all direction is different.

Fig. 10. Damage probability imaging with different PZT as transmitter.

that, when the velocity has been corrected, the imaging probability generated by a single PZT excitation can roughly describe the damage information. However, when the velocity is not corrected, the damage information of most PZT excitation is not accurate. Damage is not located in the place with high probability. On the other hand, because the velocity is faster in the ply orientation (0/90), the probability generated by a single path is not an ellipse as shown in Fig. 10 (b) but similar to a rectangle as shown in Fig. 10 (a).

The damage probability of all paths was superposed, and complete damage imaging results is obtained as shown in Fig. 11. After the velocity correction, the imaging results show the damage state of the composite plate, and the maximum probability is consistent with the damage location. When the velocity is not corrected, damage locations are incorrectly presented. It can be seen that the probability imaging method based on the velocity in all directions can identify the damage accurately for anisotropic composite plates.

4. Experimental results and discussions

To verify the effectiveness of the method, an experimental platform for ultrasonic guided waves detection of anisotropic composite plate was established. It consists of a function generator (Agilent 33522B, Palo Alto, Santa Clara County, CA, USA), an amplifier (TREK2100HF, Trek Inc., New York, NY, USA), 16-channel data acquisition card (TDEC PCI-20614, Chengdu, CN) which is composed of 4 4-channel cards and integrated on the motherboard of PC. Fig. 12 shows the connection diagram of the detection process.

A 200 kHz 5-peak sine wave modulated by Hanning window is generated by the function generator which is consistent with the simulation. The excitation signal was amplified by the amplifier to drive the PZTs to produce a strong enough signal. After complex propagation, the signals were received by data acquisition card through receiving PZTs. The used anisotropic composite plate is carbon fiber reinforced composite plastics (CFRP). The size of the

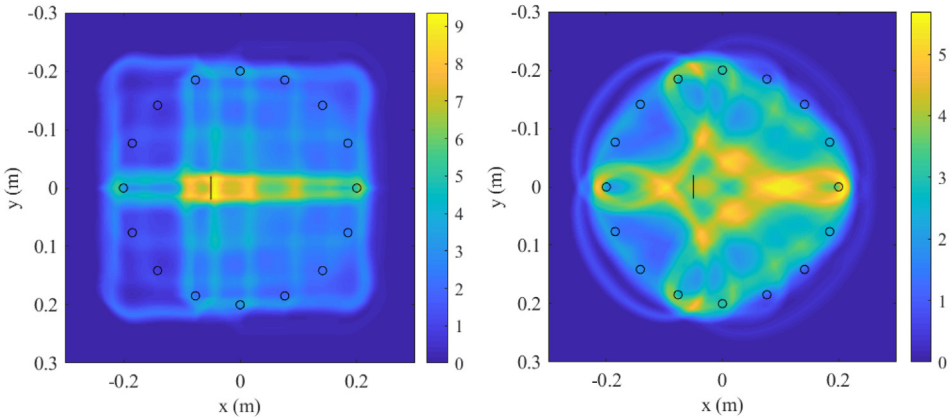

(a) Velocity in all direction is different.

(b) Velocity in all direction is the same and set to 6,969 m/s (velocity in 0 ° direction).

Fig. 11. Damage probability imaging using all paths.

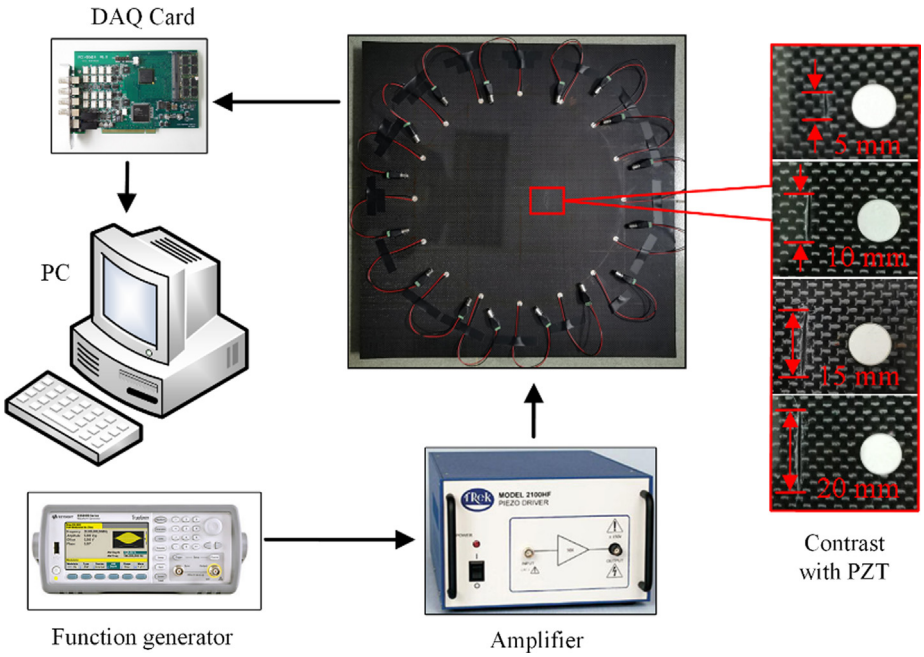

Fig. 12. The connection diagram of the detection process.

plate is 600 mm × 600 mm × 3 mm, which is the same as in the simulation. The distribution position of piezoelectric sensor and damage location are consistent with that of the simulation. The center frequency of those circular PZT are 2 MHz with 10 mm in diameter and 1 mm in thickness. To prove the effectiveness of the method, the experiments and signal acquisition were carried out for pristine and different damaged states. The states of damage include 5 mm, 10 mm, 15 mm and 20 mm, and contrast with the size of PZT as shown in Fig. 12. The sampling rate of data acquisition card is 10 MHz. 采样频率

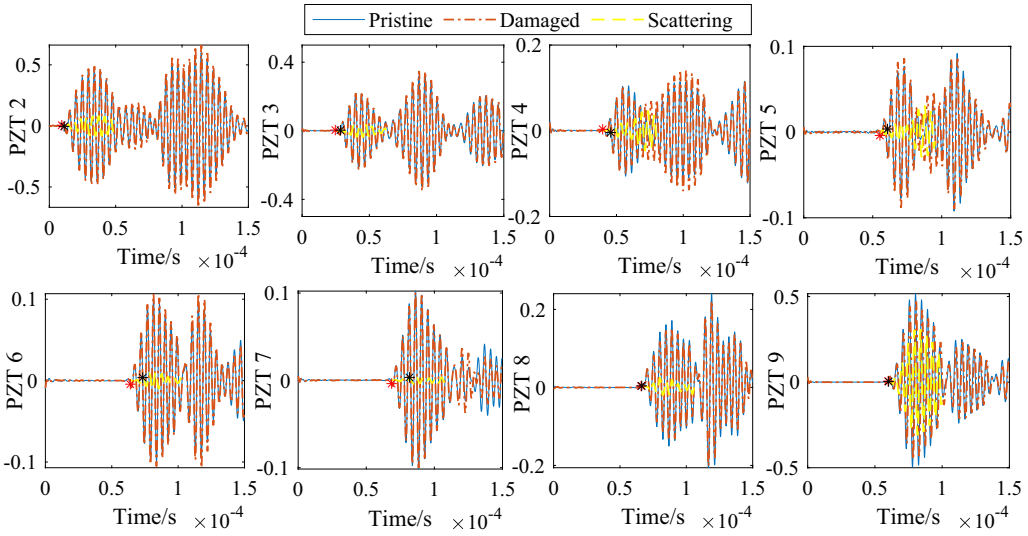

Fig. 13. The received signals from PZT 2 to 9 with PZT 1 exciting, when damage is 20 mm.

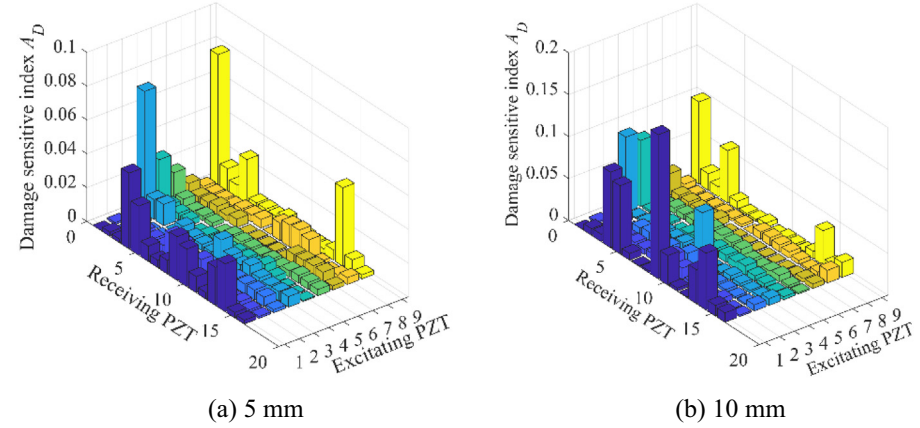

(a) 5 mm (b) 10 mm

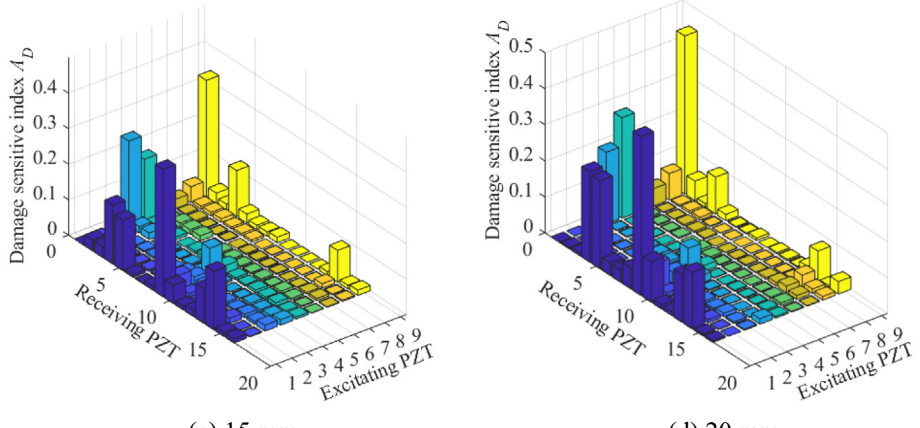

(c) 15 mm (d) 20 mm

Fig. 14. Damage sensitive index *DSI* on different damage states.

信号预处理

Because the interference of experimental data is greater than the simulation data, such as the manufacture of the plate, the consistency of the PZT and the instrument error, the experimental data are more noise. Therefore, filtering and smoothing are applied to preprocess the experimental data. Because time difference Δt, which is used for the calculation of C_T, is obtained by subtracting the arrival time of the pristine and damaged signal. The same preprocessing for the pristine and damaged signal will produce the same phase shift, which will not affect the damage location and imaging results. The cut-off frequency of the filter is 1–500 kHz, and the Gaussian smoothing with 20 window length was used. In addition, the dimensions of experiment and simulation data are inconsistent. Hence, the threshold was set to 3×10^{-3} after trial and error. Fig. 13 shows the received signals from PZT 2 to 9 after preprocess when damage is 20 mm, and PZT 1 is the excitation. *DSI* of receiving signal on path 1T-9R is largest, followed by 1T-4R and 1T-5R. Except for paths 1T-6R and 1T-7R, the value of *DSI* with PZT 1 as excitation is consistent with the simulation results, as shown in Fig. 8. The amplitude difference between two sides of the damage is not reflected. The amplitude of pristine signal is almost smaller than that of damage signal, while in the simulation, the amplitude of damaged signal received by partial PZT is obviously larger than that of pristine signal. This is because the damage production is not standardized, and the damage cannot be completely made in accordance with the simulation. In addition, the velocity in the direction of 0° (on path 1T-9R) is calculated as 6678 m / s, which is very close to the result in the velocity simulation. This further proves the correctness of the simulation.

After preprocess, C_T between different damage states and non-damage state is extracted, and *DSI* of all path were calculated. Fig. 14 shows *DSI* of different paths in different damage states. On the whole, *DSI* of different states is similar to that of the simulation which shown in Fig. 9. When the excitation is PZT 1, the value of *DSI* on path 1T-9R is the largest, followed by paths 1T-4R and 1T-5R, and the value of *DSI* on paths 1T-14R and 1T-13R which are symmetrical with paths 1T-4R and 1T-5R is also large. When the excitation is PZT 2 and 3, the values of *DSI* are not much different, and only when PZT 9 is the receiver, it is slightly larger than other paths. When the excitation is PZT 4, the value of *DSI* on path 4T-1R and 4T-9R is the larger, and other paths are smaller. When the excitation is PZT 5, 6, 7 and 8, the values of *DSI* are small except for PZT 1 as the receiver, and among them, the value of *DSI* on path 5T-1R is the largest. When the excitation is PZT 9, the value of *DSI* on path 9T-1R is the largest, followed by paths 9T-4R, and the value of *DSI* on path 9T-14R which are symmetrical with path 9T-4R is also large. It can be seen that *DSI* is more sensitive to the damage in the region formed by the exciting and receiving PZT. For example, the difference between paths 2T-9R, 3T-9R and 6T-1R, 7T-1R, 8T-1R. On the other hand, the actual location of the damage is on the path of PZT 1 and 9, and between PZT 4, 5 or PZT 14, 13. The value of *DSI* is large when PZT 1, 4, 5, 9, 13 and 14 are receiver.

Moreover, on the main path, the value of *DSI* increases with the increase of damage degree. However, it is not very accurate to evaluate the damage state of the composite plate only through one path. The sum of damage sensitive index DSI_{sum} was used to assess the damage degree of material, and a damage threshold *DT* is set to 0.3. The value of *DT* is determined by calculated DSI_{sum} of non-damaged and damaged state. The value of DSI_{sum} on different damage states (5 mm, 10 mm, 15 mm and 20 mm) is 0.9929, 1.6603, 3.1091 and 3.3454 respectively, which exceeded the damage

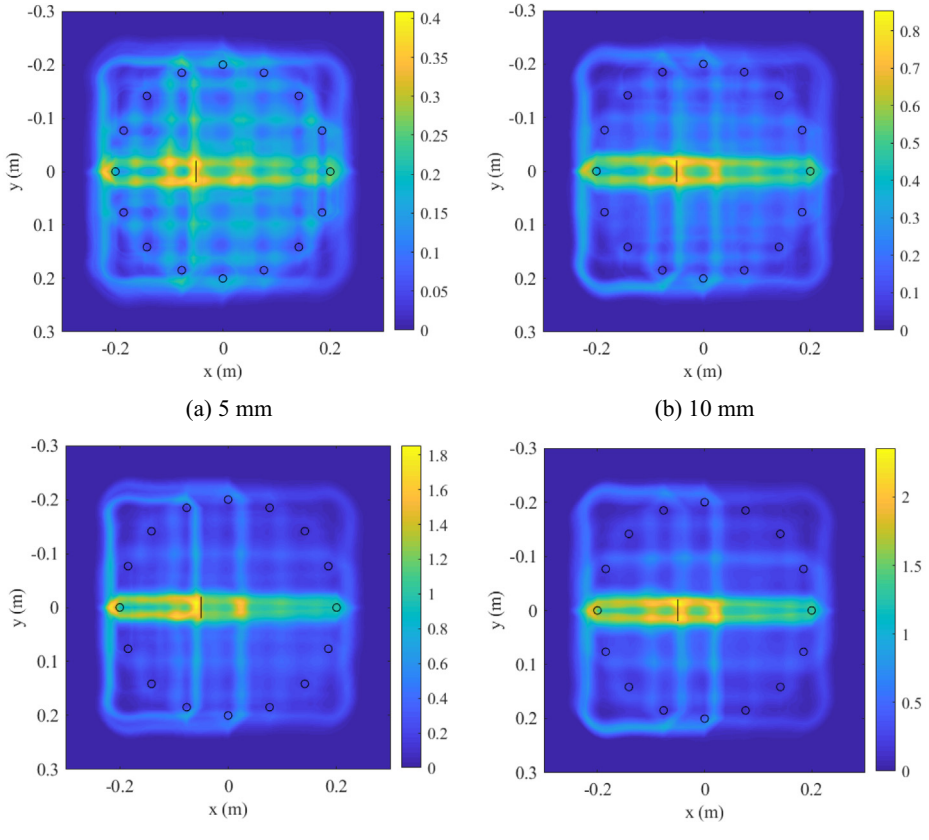

Fig. 15. Damage probability imaging of experimental data on different damage states.

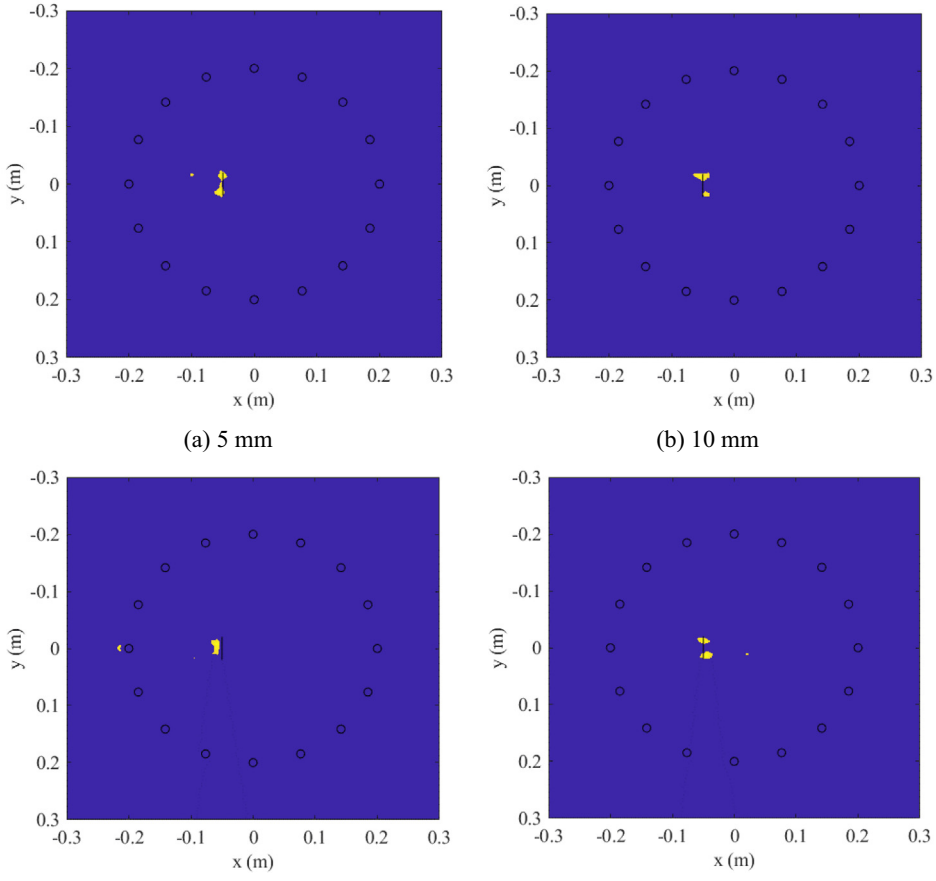

Fig. 16. Damage probability imaging of experimental data on different damage states with a threshold of *IT* = 90%.

本文创新点？

threshold, indicating that there was damage. Meanwhile, the value of DSI_{sum} also increases with the damage degree, which means it can reflect the severity of the damage.

According to C_T and *DSI* of all paths, the probability of the plate is calculated, and present the result in the form of images. Fig. 15 shows the damage probability imaging of experimental data on different damage states 5 mm, 10 mm, 15 mm and 20 mm. Theoretically, the damage may be outside the range of PZT configuration, so the imaging area is not limited. The damage position in all damage state is clear at a glance, and the position is accurately described by the maximum probability. But there is another high probability location near the damage. This is because the actual position of the damage is between PZT 4, PZT 5 or PZT 14, 13. When PZT 4, and 14 are receivers, the maximum probability appears at the actual location of the damage, while when PZT 5, and 13 are receivers, the maximum probability appears near the actual location of the damage. In addition, when a PZT is the excitation, 15 paths formed by it and other remaining PZTs are all around the PZT, so a large probability value will also be generated near the excitation PZT, resulting in imaging error. This is how a large probability is generated near PZT 1. To reduce these interferences and make the imaging results more intuitive, an imaging threshold *IT* can be applied. Fig. 16 shows the improved image with *IT* = 90%. The location of the damage is very clear, although there is a little interference. The probability is higher at both ends of the crack than in the middle, which is the reason why one crack is divided into two damage. In fact, it more accurately reflects the influence of crack damage on the received signal, because the scattering signal of the guided waves at the crack tip is the most obvious.

5. Conclusions

This paper developed a velocity anisotropy probability imaging method by ultrasonic guided waves to improve the imaging quality composite plates. Simulations and experiments were carried out to verify the feasibility and effectiveness of the method. The main contributions of the paper are concluded as follows:

(1) The velocity of all directions is different due to anisotropy. The larger the Angle between the propagation direction and the ply direction, the slower the velocity of the guided waves will be. This is consistent with the characteristic of the composite plates.
(2) C_T between damage and reference point is employed to determine damage location. The scaling coefficient γ is defined to control the attenuation speed of probability, and a good imaging effect is obtained when it is set to 0.1. β=0.1
(3) *DSI* shows a similar trend in different damage degree, except for the obvious difference in magnitude. The value of *DSI* associated with the damage path is larger, and it can be used to characterize the amplitude of the damage probability.
(4) DSI_{sum} of all damage states (5 mm, 10 mm, 15 mm and 20 mm) exceeded the damage threshold and increases with the damage degree. It can indicate the severity of the damage.
(5) This method can accurately show the damage location under different damage degree, the damage location is clearer by applying a threshold of 90%. The probability is higher at

crack tips, which more accurately reflects the influence of crack damage on the received signal.

In summary, the proposed probability imaging method based on the velocity of all directions can accurately present damage state. The damage degree and location can be accurately described. The damage imaging quality is improved by using the velocity in all directions. However, only one single damage is considered in this paper. The next step is to study multi damage imaging, and the extraction method of time coefficient and damage sensitive index could be improved for such complex problems.

CRediT authorship contribution statement

Yuan Liu: Conceptualization, Methodology, Software, Investigation, Resources, Formal analysis, Writing - original draft. **Xiaobin Hong:** Conceptualization, Supervision, Project administration, Supervision, Writing - review & editing, Visualization. **Bin Zhang:** Resources, Validation, Formal analysis, Software, Writing - review & editing, Visualization.

Declaration of Competing Interest

The authors declare that they have no known competing financial interests or personal relationships that could have appeared to influence the work reported in this paper.

Acknowledgements

This work is supported by the National Natural Science Foundation of China under grant No. 51975220, Natural Science Foundation of Guangdong Province under grant No. 2019B151502057, Guangdong Province Science & Technology project under grant No. 2018B010109004 and 2018B010109005, Guangzhou Science & Technology project under grant No. 201902010024 and 201802020021, the Fundamental Research Funds for the Central Universities project under grant No. 2019ZD23.

References

[1] J. Vishnuvardhan, A. Muralidharan, C.V. Krishnamurthy, K. Balasubramaniam, Structural health monitoring of anisotropic plates using ultrasonic guided wave STMR array patches, NDT E Int. 42 (3) (2009) 193–198.
[2] L. Yu, V. Giurgiutiu, In situ 2-D piezoelectric wafer active sensors arrays for guided wave damage detection, Ultrasonics 48 (2) (2008) 117–134.
[3] J.S. Hall, P. Fromme, J.E. Michaels, Guided wave damage characterization via minimum variance imaging with a distributed array of ultrasonic sensors, J. Nondestr. Eval. 33 (3) (2014) 299–308.
[4] Z. Tian, L. Yu, C. Leckey, Rapid guided wave delamination detection and quantification in composites using global-local sensing, Smart Mater. Struct. 25 (8) (2016) 085042.
[5] J.S. Hall, J.E. Michaels, Computational efficiency of ultrasonic guided wave imaging algorithms, IEEE Trans. Ultrason. Ferroelectr. Freq. Control 58 (1) (2011) 244–248.
[6] Z. Sharif-Khodaei, M.H. Aliabadi, Assessment of delay-and-sum algorithms for damage detection in aluminium and composite plates, Smart Mater. Struct. 23 (7) (2014) 075007.
[7] G. Lu, Y. Li, T. Wang, H. Xiao, L. Huo, G. Song, A multi-delay-and-sum imaging algorithm for damage detection using piezoceramic transducers, J. Intell. Mater. Syst. Struct. 28 (9) (2017) 1150–1159.
[8] D. Wang, L. Ye, Z. Su, Y. Lu, F. Li, G. Meng, Probabilistic damage identification based on correlation analysis using guided wave signals in aluminum plates, Struct. Health Monit. 9 (2) (2010) 133–144.
[9] J. Hettler, M. Tabatabaeipour, S. Delrue, K. Van Den Abeele, Linear and nonlinear guided wave imaging of impact damage in CFRP using a probabilistic approach, Materials 9 (11) (2016) 901.
[10] D. Li, H. Yu, F. Xu, J.Q. Zhang, An lp-norm approach to robust probabilistic inspection of plate-like structure defects with guided waves, Smart Mater. Struct. 26 (10) (2017) 104003.
[11] C. Zhou, Z. Su, L. Cheng, Probability-based diagnostic imaging using hybrid features extracted from ultrasonic Lamb wave signals, Smart Mater. Struct. 20 (12) (2011) 125005.
[12] Z. Su, M. Hong, Nonlinear ultrasonics for health monitoring of aerospace structures using active sparse sensor networks. In Structural Health Monitoring (SHM) in Aerospace Structures, Woodhead Publishing, 2016, pp. 353–392.
[13] X. Liu, L. Bo, K. Yang, Y. Liu, Y. Zhao, J. Zhang, et al., Locating and imaging contact delamination based on chaotic detection of nonlinear lamb waves, Mech. Syst. Sig. Process. 109 (2018) 58–73.
[14] L. Zeng, L. Huang, J. Lin, Damage imaging of composite structures using multipath scattering Lamb waves, Compos. Struct. 216 (2019) 331–339.
[15] J. Moll, R.T. Schulte, B. Hartmann, C.P. Fritzen, O. Nelles, Multi-site damage localization in anisotropic plate-like structures using an active guided wave structural health monitoring system, Smart Mater. Struct. 19 (4) (2010) 045022.
[16] T. Kundu, S. Das, S.A. Martin, K.V. Jata, Locating point of impact in anisotropic fiber reinforced composite plates, Ultrasonics 48 (3) (2008) 193–201.
[17] V. Sethi, G. Song, Multimodal vibration control of a flexible structure using piezoceramic sensor and actuator, J. Intell. Mater. Syst. Struct. 19 (5) (2008) 573–582.
[18] L.S. Jang, K.C. Kuo, Fabrication and characterization of PZT thick films for sensing and actuation, Sensors 7 (4) (2007) 493–507.
[19] Y. Shen, V. Giurgiutiu, Predictive modeling of nonlinear wave propagation for structural health monitoring with piezoelectric wafer active sensors, J. Intell. Mater. Syst. Struct. 25 (4) (2014) 506–520.
[20] J. Wang, Y. Shen, An enhanced Lamb wave virtual time reversal technique for damage detection with transducer transfer function compensation, Smart Mater. Struct. 28 (8) (2019) 085017.
[21] W.T. Peter, X. Wang, Characterization of pipeline defect in guided-waves based inspection through matching pursuit with the optimized dictionary, NDT and E Int. 54 (2013) 171–182.
[22] S.M. Parvasi, S.C.M. Ho, Q. Kong, R. Mousavi, G. Song, Real time bolt preload monitoring using piezoceramic transducers and time reversal technique—A numerical study with experimental verification, Smart Mater. Struct. 25 (8) (2016) 085015.
[23] T. Jiang, Y. Zhang, L. Wang, L. Zhang, G. Song, Monitoring fatigue damage of modular bridge expansion joints using piezoceramic transducers, Sensors 18 (11) (2018) 3973.
[24] X. Hong, X. Lin, B. Yang, M. Li, Crack detection in plastic pipe using piezoelectric transducers based on nonlinear ultrasonic modulation, Smart Mater. Struct. 26 (10) (2017) 104012.
[25] X. Hong, Y. Liu, P. Lin, W. Xu, Interfacial Adhesion-strength detection of structural silicone sealant for hidden frame-supported glass curtain wall based on nonlinear ultrasonic lamb wave, J. Aerosp. Eng. 31 (5) (2018) 04018047.
[26] X. Hong, Y. Liu, Y. Liufu, P. Lin, Debonding detection in hidden frame supported glass curtain walls using the nonlinear ultrasonic modulation method with piezoceramic transducers, Sensors 18 (7) (2018) 2094.
[27] X. Hong, J. Zhou, Y. He, Damage detection of anchored region on the messenger cable based on matching pursuit algorithm, Mech. Syst. Sig. Process. 130 (2019) 221–247.
[28] X. Hong, B. Zhang, Y. Liu, Z. Zhou, M. Ye, H. Qi, Liquid level detection in porcelain bushing type terminals using piezoelectric transducers based on auto-encoder networks, Measurement 141 (2019) 12–23.
[29] M. Luo, W. Li, C. Hei, G. Song, Concrete infill monitoring in concrete-filled FRP tubes using a PZT-based ultrasonic time-of-flight method, Sensors 16 (12) (2016) 2083.
[30] A. Velichko, P.D. Wilcox, Modeling the excitation of guided waves in generally anisotropic multilayered media, J. Acoust. Soc. Am. 121 (1) (2007) 60–69.
[31] E. Glushkov, N. Glushkova, A. Eremin, R. Lammering, Group velocity of cylindrical guided waves in anisotropic laminate composites, J. Acoust. Soc. Am. 135 (1) (2014) 148–154.
[32] Y. Shen, C.E.S. Cesnik, Hybrid local fem/global lisa modeling of damped guided wave propagation in complex composite structures, Smart Mater. Struct. 25 (9) (2016) 095021.
[33] J.E. Michaels, Detection, localization and characterization of damage in plates with an in situ array of spatially distributed ultrasonic sensors, Smart Mater. Struct. 17 (3) (2008) 035035.
[34] J.S. Hall, J.E. Michaels, Minimum variance ultrasonic imaging applied to an in situ sparse guided wave array, IEEE Trans. Ultrason. Ferroelectr. Freq. Control 57 (10) (2010) 2311–2323.
[35] X. Chen, J.E. Michaels, T.E. Michaels, A methodology for estimating guided wave scattering patterns from sparse transducer array measurements, IEEE Trans. Ultrason. Ferroelectr. Freq. Control 62 (1) (2015) 208–219.
[36] G. Lu, Y. Li, G. Song, A delay-and-Boolean-ADD imaging algorithm for damage detection with a small number of piezoceramic transducers, Smart Mater. Struct. 25 (9) (2016) 095030.
[37] M. Hong, Z. Su, Y. Lu, H. Sohn, X. Qing, Locating fatigue damage using temporal signal features of nonlinear Lamb waves, Mech. Syst. Sig. Process. 60 (2015) 182–197.